Available online at www.sciencedirect.com
SCIENCE DIRECT®
Progress in Oceanography 64 (2005) 307–324
Progress in Oceanography
www.elsevier.com/locate/pocean

Simulated biogeochemical responses to iron enrichments in three high nutrient, low chlorophyll (HNLC) regions

Masahiko Fujii [a,*], Naoki Yoshie [b], Yasuhiro Yamanaka [b,c], Fei Chai [a]

[a] School of Marine Sciences, 5741 Libby Hall, University of Maine, Orono, ME 04469, USA
[b] Graduate School of Environmental Earth Science, Hokkaido University, N10W5, Kita-ku, Sapporo 060-0810, Japan
[c] Ecosystem Change Research Program, Frontier Research System for Global Change, 3173-25 Showa-machi, Kanazawa-ku, Yokohama 236-0001, Japan

Available online 7 April 2005

Abstract

To fill temporal gaps in iron-enrichment experimental data and gain further understanding of marine ecosystem responses to iron enrichments, we apply a fifteen-compartment ecosystem model to three iron-enrichment sites, namely SEEDS (the Subarctic Pacific Iron Experiment for Ecosystem Dynamics Study; 48.5°N, 165°E) in the western North Pacific, SOIREE (the Southern Ocean Iron RElease Experiment; 61°S, 140°E) in the Southern Ocean, and IronExII (the second mesoscale iron enrichment experiment; 3.5°S, 104°W) in the Equatorial Pacific. The ecological effects of iron in the model are represented by changing two photosynthetic parameters during the iron-enrichment period. The model results successfully reproduce the observed biogeochemical responses inside and outside the iron patch at each site, such as rapid increases in plankton biomass and biological productivity, and decreases in surface nutrients and pCO_2, inside the patch. However, the modeled timing and magnitude of changes differ among the sites because of differences in both physical environments and plankton species. After the iron enrichment, the diatom productivity is strongly controlled by light at SOIREE and by silicate at IronExII and SEEDS. Light limitation due to self-shading by the phytoplankton is significant during the bloom at all sites. Sensitivity analysis of the model results to duration of the iron enrichment reveals that long-term multiple infusions over more than a week would not be effective at SEEDS because of strong silicate limitation on diatom growth. Sensitivity of the model to water temperature shows that export production is higher at lower temperatures, because of slower recycling of particulate organic carbon. Therefore, the e-ratio (the ratio of export production to primary production) is inversely correlated with temperature, and the relationship can be described with a linear function. Through this study, we conclude that ecosystem modeling is a powerful tool to help design future iron-enrichment experiments and observational plans.

Keywords: Modelling; High nutrient low chlorophyll (HNLC) regions; Algal bloom; Limiting factors; Water temperature; Remineralization

* Corresponding author. Tel.: +1 207 581 4338; fax: +1 207 581 4990.
E-mail address: mfujii@maine.edu (M. Fujii).

0079-6611/$ - see front matter © 2005 Elsevier Ltd. All rights reserved.
doi:10.1016/j.pocean.2005.02.017

1. Introduction

The North Pacific, the Southern Ocean and the Equatorial Pacific are known as major high-nutrient, low-chlorophyll (HNLC) regions in which biological productivity is lower than expected for the prevailing surface nutrient conditions. Martin (1990) suggested that the relatively low productivity in the HNLC regions is due to low surface iron concentration, since iron is one of the essential micronutrients for many phytoplankton species. To elucidate Martin's hypothesis, several open ocean iron enrichment experiments have been conducted in the HNLC regions. The manifestation of these in situ iron enrichments is increase in surface chlorophyll-*a*, enhanced biological productivity, drawdown in surface nutrients and decrease in surface pCO_2. However, logistic constraints on the length of time research vessels can remain with the fertilized patch have limited these experiments to about 20 days, not long enough for significant changes occur at high trophic levels. In addition, what is not yet well documented is the fate of the iron-stimulated productivity once it disappears from the euphotic zone (Charette & Buesseler, 2000; Ridgwell, 2000), i.e., how much of it is transported vertically out of the euphotic zone. Therefore, it is useful to investigate gaps in the field observations, with numerical model simulations. Ecosystem modeling can also help us interpret the observed results. For these purposes, several ecosystem models have been applied to the iron-enriched sites and have produced realistic results.

Using an ecosystem model including cycling of the iron, Hannon, Boyd, Silvoso, and Lancelot (2001) realistically reproduced ecological responses to the iron infusion for SOIREE (the Southern Ocean Iron RElease Experiment; from 9 to 22 February 1999 at 61°S, 140°E) in the Southern Ocean. They concluded that 13 days of observation are not long enough to capture the entire phytoplankton bloom period and subsequent increase in the downward particulate organic carbon (POC) flux. By changing the photosynthetic efficiency and nutrient uptake kinetics of the phytoplankton in an ecosystem model (Chai, Dugdale, Peng, Wilkerson, & Barber, 2002) to reflect the effects of the iron infusion, Chai, Jiang, Barber, and Chavez (submitted) successfully reproduced the observed ecological responses to the iron infusion for the IronExII (the second mesoscale iron enrichment experiment; from 29 May to 16 June 1995 at 3.5°S, 104°W) in the Equatorial Pacific. They indicate that it takes more than one month for detrital siliceous materials to sink out of the euphotic zone. Yoshie, Fujii, and Yanamaka (2005) introduced two species of diatoms to their ecosystem model and obtained realistic results in the biogeochemical responses to the SEEDS (the Subarctic Pacific Iron Experiment for Ecosystem Dynamics Study; from 18 to 31 July 2001 at 48.5°N, 165°E) iron infusion in the western North Pacific. By dividing diatoms into two species in the model, they successfully reproduced the timing of the observed sudden diatom bloom that started five days after the iron enrichment.

In this study, we use an ecosystem model to simulate biogeochemical responses to iron enrichments in three HNLC regions with the objectives (1) to fill the gaps in the observational data and gain further understanding of multiple, open-ocean iron-enrichment experiments, (2) to compare similarities and differences in biogeochemical responses to iron enrichment among different experiments, and (3) to perform sensitivity studies and obtain information for planning future iron-enrichment experiments. We apply an ecosystem model to three iron-infusion experimental sites, namely SEEDS, SOIREE and IronExII. Comparison of the model results among these three sites enables us to identify how differences in both physical environment and plankton physiology affect biogeochemical responses to the iron infusion. We investigate what factors constrain biological productivity at each site once the iron limitation is alleviated. Sensitivity of the model to duration of the iron infusion and to water temperature at SEEDS is analyzed.

2. Model description and experimental design

A fifteen-compartment marine ecosystem model (Fig. 1; Fujii, Nojiri, Yamanaka, & Kishi, 2002; Yamanaka, Yoshie, Fujii, Aita, & Kishi, 2004) is applied to SEEDS, SOIREE and IronExII. A few

modifications of the ecosystem model from the previous studies are carried out to apply the model globally (Aita, Yamanaka, & Kishi, 2003). The Steele-type light dependency of phytoplankton photosynthesis (Steele, 1962) is replaced with the Platt-type (Platt, Gallegos, & Harrison, 1980). The dependency of phytoplankton physiologies, i.e., photosynthesis, respiration, extracellular excretion and mortality, on the temperature changes to a factor of 1.48 for each 10 °C ($Q_{10} = 1.48$; Suzuki & Takahashi, 1995) instead of $Q_{10} = 2.0$ (doubling).

The primary productivity by non-diatom small phytoplankton (PS) and diatoms (PL) in the model (PP_{PS} and PP_{PL} hereafter) depend upon the concentration of nitrogenous nutrients (nitrate and ammonium), the temperature and the light. The PP_{PL} also depends upon the silicate concentration. Hence, PP_{PS} and PP_{PL} in the model are described as follows:

$$PP_{PS} = V_{\max S} \times \underbrace{\left\{ \frac{[NO_3]}{[NO_3] + K_{NO_{3S}}} \exp(-\Psi_S \times [NH_4]) + \frac{[NH_4]}{[NH_4] + K_{NH_{4S}}} \right\}}_{\text{nitrogenous dependency}} \times \underbrace{\exp(k_S T)}_{\text{temperature dependency}} \times \underbrace{\left\{ 1 - \exp\left(-\frac{\alpha_S \times I}{V_{\max S}} \right) \right\}}_{\text{light dependency}} \times [PS] \tag{1}$$

and

$$PP_{PL} = V_{\max L} \times \min \left\{ \underbrace{\frac{[NO_3]}{[NO_3] + K_{NO_{3L}}} \exp(-\Psi_L \times [NH_4]) + \frac{[NH_4]}{[NH_4] + K_{NH_{4L}}}}_{\text{nitrogenous dependency}}, \underbrace{\frac{[Si]}{[Si] + K_{Si\,L}}}_{\text{silicate dependency}} \right\} \times \underbrace{\exp(k_L T)}_{\text{temperature dependency}} \times \underbrace{\left\{ 1 - \exp\left(-\frac{\alpha_L \times I}{V_{\max L}} \right) \right\}}_{\text{light dependency}} \times [PL], \tag{2}$$

where T is the water temperature, I is the solar radiation.

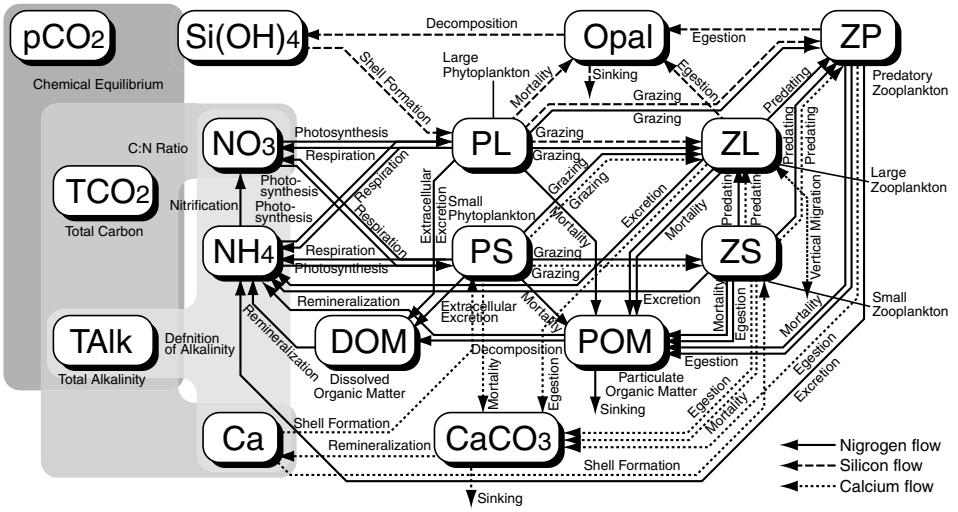

Fig. 1. Schematic view of a fifteen-compartment marine ecosystem model (from Fujii et al., 2002; Yamanaka et al., 2004).

Remineralization of particulate organic matter (particulate organic nitrogen (PON) or POC) in the model is assumed to obey first kinetics as follows:

$$\text{POM remineralization} = V_{\text{PD10}} \times \exp(k_{\text{PD}} T) \times [\text{POM}]. \quad (3)$$

Species of in situ phytoplankton and zooplankton differ among these three iron-enrichment sites. They are categorized in the model as shown in Table 1. The parameters and their values used in the model are listed in Table 2. Most of the parameter values are the same for all three sites, except values of the maximum grazing rates by ZL at IronExII are modified so that the model results can better reproduce the IronExII observations. Values of the maximum photosynthetic rate of PL ($V_{\max L}$) and the initial slope of P–I curve for PL (α_L) in the model are set to increase by three times during first few days of the iron infusion (Fig. 2), similar to the procedure used by Chai et al. (submitted). At SOIREE and IronExII, the values of the maximum photosynthetic rate and the initial slope of P–I curve for PS ($V_{\max S}$ and α_S, respectively), in addition to the increases for the diatom growth parameters, are also set to increase by three times during the initial iron infusion period (Fig. 2). This is done considering the observed results that not only diatoms but also non-diatom small phytoplankton bloom immediately after the iron infusion at these two sites (Hall & Safi, 2001; Hannon et al., 2001; Landry et al., 2000). In the model, the duration for which these parameter values are kept at their highest levels is set to seven days at all sites, then decreases to the normal values at Day 20 after the first day of the iron infusion (Fig. 2). Only the SEEDS experiment resulted in transition of the dominant diatom species from pennate diatoms to a centric diatom, *Chaetoceros debilis*, at the beginning of the iron enrichment (Tsuda et al., 2003). An argument about the increase in the diatom growth parameter values has been developed in Yoshie et al. (2005). The carbon-chlorophyll-*a* ratio by weight inside and outside the patch in the model is fixed to 50 and 50 at SEEDS, 74 and 105 at SOIREE, and 92 and 170 at IronExII, respectively, according to the observed results.

The ecosystem model is coupled with a one-dimensional mixed layer model. The physical model has 20 layers in the vertical, which provides a resolution of 5 m spanning a model domain from the surface to 100 m depth. The vertical velocity is taken to be zero. All the iron-enrichment experiments are carried out in summer when the surface layer is sufficiently stratified. The mixed layer depth is set to 25 m at SEEDS, 65 m at SOIREE and 37.5 m at IronExII for simplicity in the model. The vertical diffusive coefficient is given so as to reproduce the observed temperature and salinity (Yoshie et al., 2005), and is set to 0.4 $\text{cm}^2\ \text{s}^{-1}$ below the mixed layer at each experimental site.

This study focuses on comparing modeled differences in response to the iron enrichments among three sites. For this purpose, we use simplified physical forcings to drive the model so that the biogeochemical differences can arise from differences in very general physical environments and biogeochemical processes.

Table 1
Phytoplankton and zooplankton in each iron-enrichment site categorized in the model

	SEEDS	SOIREE	IronExII
Large phytoplankton (PL)	Centric diatom *Chaetoceros debilis*	Diatoms	Diatoms
Small phytoplankton (PS)	The other smaller phytoplankton	Autotrophic nanoflagellates	The other smaller phytoplankton
Predatory zooplankton (ZP)	Carnivorous *Chaetogratha*	Carnivorous mesozooplankton	Carnivorous mesozooplankton
Large zooplankton (ZL)	Copepoda	Ciliates	Heterotrophic dinoflagellates and ciliates
Small zooplankton (ZS)	The other smaller zooplankton	Heterotrophic flagellates	The other smaller zooplankton
References	Saito et al. (2005) Tsuda et al. (2005)	Hall and Safi (2001) Hannon et al. (2001)	Landry et al. (2000) Rollwagen Bollens and Landry (2000)

Table 2
List of parameter values

Parameters	Symbol	Value	Unit	Source
(*for underwater light dissipation*)				
Light dissipation coefficient of sea water	α_1	0.04	m^{-1}	(1)
Self-shading coefficient by phytoplankton	α_2	0.04	$\mu mol\ N^{-1}\ l\ m^{-1}$	(1)
(*for PS*)				
Initial slope of *P–I* curve	α_s	0.025	$day^{-1}\ W^{-1}\ m^2$	(2)
Maximum photosynthetic rate at 10 °C	$V_{max\,S}$	0.592	day^{-1}	(3)
Half saturation constant for NO_3	k_{NO3S}	3.0	$\mu mol\ N\ l^{-1}$	(4)
Half saturation constant for NH_4	k_{NH4S}	0.3	$\mu mol\ N\ l^{-1}$	(4)
NH_4 inhibition rate	Ψ_S	1.5	$\mu mol\ N^{-1}$	(4)
Temperature coefficient for photosynthetic rate	k_S	0.0392	$°C^{-1}$	(5)
Mortality rate at 10 °C	M_{PS10}	0.087	$\mu mol\ N^{-1}\ 1\ day^{-1}$	(4)
Temperature coefficient for mortality	k_{MPS}	0.0392	$°C^{-1}$	(5)
Respiration rate at 10 °C	R_{S10}	0.044	day^{-1}	(4)
Temperature coefficient for respiration	k_{RS}	0.0392	$°C^{-1}$	(5)
Ratio of extracellular excretion to photosynthesis	γ_S	0.135	No dimension	(4)
(*for PL*)				
Initial slope of *P–I* curve	α_L	0.025	$day^{-1}\ W^{-1}\ m^2$	(2)
Maximum photosynthetic rate at 10 °C	$V_{max\,L}$	1.184	day^{-1}	(3)
Half saturation constant for NO_3	k_{NO3L}	3.0	$\mu mol\ N\ l^{-1}$	(4)
Half saturation constant for NH_4	k_{NH4L}	0.3	$\mu mol\ N\ l^{-1}$	(4)
NH_4 inhibition rate	Ψ_L	1.5	$\mu mol\ N^{-1}$	(4)
Half saturation constant for Si	k_{Si}	3.0	$\mu mol\ Si\ l^{-1}$	(3)
Temperature coefficient for photosynthetic rate	k_L	0.0392	$°C^{-1}$	(5)
Mortality rate at 10 °C	M_{PL10}	0.087	$\mu mol\ N^{-1}\ 1\ day^{-1}$	(3)
Temperature coefficient for mortality	k_{MPL}	0.0392	$°C^{-1}$	(5)
Respiration rate at 10 °C	R_{L10}	0.044	day^{-1}	(4)
Temperature coefficient for respiration	k_{RL}	0.0392	$°C^{-1}$	(5)
Ratio of extracellular excretion to photosynthesis	γ_L	0.135	No dimension	(4)
(*for ZS*)				
Maximum rate of grazing PS at 10 °C	$G_{RmaxS,PS}$	0.8	day^{-1}	(4)
Temperature coefficient for grazing	k_{GS}	0.0693	$°C^{-1}$	(4)
Ivlev constant	λ_S	1.4	$\mu mol\ N^{-1}$	(4)
Threshold value for grazing PS	PS^*_{ZS}	0.043	$\mu mol\ N\ l^{-1}$	(4)
Assimilation efficiency	α_{ZS}	0.7	No dimension	(4)
Growth efficiency	β_{ZS}	0.3	No dimension	(4)
Mortality rate at 10 °C	M_{ZS10}	0.12	$\mu mol\ N^{-1}\ 1\ day^{-1}$	(4)
Temperature coefficient for mortality	k_{ZS}	0.0693	$°C^{-1}$	(4)
(*for ZL*)				
Maximum rate of grazing PS at 10 °C	$G_{RmaxL,PS}$	0.2 (SEEDS, SOIREE)	day^{-1}	(4)
		0.8 (IronExII)		(3)
Maximum rate of grazing PL at 10 °C	$G_{RmaxL,PL}$	0.8 (SEEDS, SOIREE)	day^{-1}	(4)
		0.2 (IronExII)		(3)
Maximum rate of predating ZS at 10 °C	$G_{RmaxL,ZS}$	0.8 (SEEDS, SOIREE)	day^{-1}	(4)
		0.4 (IronExII)		(3)
Temperature coefficient for grazing/predation	k_{GL}	0.0693	$°C^{-1}$	(4)
Ivlev constant	λ_L	1.4	$\mu mol\ N^{-1}$	(4)
Threshold value for grazing PS	PS^*_{ZL}	0.043	$\mu mol\ N\ l^{-1}$	(4)
Threshold value for grazing PL	PL^*_{ZL}	0.043	$\mu mol\ N\ l^{-1}$	(4)
Threshold value for predating ZS	ZS^*_{ZL}	0.043	$\mu mol\ N\ l^{-1}$	(4)
Assimilation efficiency	α_{ZL}	0.7	No dimension	(4)
Growth efficiency	β_{ZL}	0.3	No dimension	(4)

(*continued on next page*)

Table 2 (*continued*)

Parameters	Symbol	Value	Unit	Source
Mortality rate at 10 °C	M_{ZL10}	0.12	μmol N^{-1} 1 day^{-1}	(4)
Temperature coefficient for mortality	k_{ZL}	0.0693	$°C^{-1}$	(4)
(*for ZP*)				
Maximum rate of grazing PL at 10 °C	$G_{RmaxP,PL}$	0.4	day^{-1}	(4)
Maximum rate of predating ZS at 10 °C	$G_{RmaxP,ZS}$	0.4	day^{-1}	(3)
Maximum rate of predating ZL at 10 °C	$G_{RmaxP,ZL}$	0.8	day^{-1}	(3)
Temperature coefficient for grazing/predation	k_{GP}	0.0693	$°C^{-1}$	(4)
Ivlev constant	λ_P	1.4	μmol N^{-1}	(4)
Threshold value for grazing PL	PL^*_{ZP}	0.043	μmol N l^{-1}	(4)
Threshold value for predating ZS	ZS^*_{ZP}	0.043	μmol N l^{-1}	(4)
Threshold value for predating ZL	ZL^*_{ZP}	0.043	μmol N l^{-1}	(4)
Preference coefficient for PL	Ψ_{PL}	4.6	μmol N^{-1}	(4)
Preference coefficient for ZS	Ψ_{ZS}	3.0	μmol N^{-1}	(4)
Assimilation efficiency	α_{ZP}	0.7	No dimension	(4)
Growth efficiency	β_{ZP}	0.3	No dimension	(4)
Mortality rate at 10 °C	M_{ZP10}	0.47	μmol N^{-1} 1 day^{-1}	(3)
Temperature coefficient for mortality	k_{ZP}	0.0693	$°C^{-1}$	(4)
(*for nitrification*)				
Nitrification rate at 10 °C	N_{it10}	0.06	day^{-1}	(4)
Temperature coefficient for nitrification	k_{Nit}	0.0693	$°C^{-1}$	(4)
(*for sinking and decomposition*)				
PON sinking velocity	S_{PON}	40.0	m day^{-1}	(4)
Decomposition rate of PON to DON at 10 °C	V_{PD10}	0.2	day^{-1}	(4)
Temperature coefficient for PON decomposition to DON	k_{PD}	0.0693	$°C^{-1}$	(4)
Decomposition rate of PON to NH_4 at 10 °C	V_{PA10}	0.2	day^{-1}	(4)
Temperature coefficient for PON decomposition to NH_4	k_{PA}	0.0693	$°C^{-1}$	(4)
Decomposition rate of DON to NH_4 at 10 °C	V_{DA10}	0.4	day^{-1}	(1)
Temperature coefficient for DON decomposition to NH_4	k_{DA}	0.0693	$°C^{-1}$	(4)
Opal sinking velocity	S_{Opal}	40.0	m day^{-1}	(4)
Decomposition rate of Opal at 10 °C	V_{Opal}	0.2	day^{-1}	(4)
Temperature coefficient for Opal decomposition	k_{Opal}	0.0693	$°C^{-1}$	(4)
$CaCO_3$ sinking velocity	S_{CaCO3}	40.0	m day^{-1}	(4)
Decomposition rate of $CaCO_3$ at 10 °C	V_{CaCO3}	0.1	day^{-1}	(4)
Temperature coefficient for $CaCO_3$ decomposition	k_{CaCO3}	0.0693	$°C^{-1}$	(4)
(*for each ratio*)				
Stoichiometry of carbon to nitrogen	R_{CN}	6.625	No dimension	(4)
PL stoichiometry of silicon to nitrogen	R_{SiN}	2.0	No dimension	(4)
Ratio of cocolithophorids to PS	R_{coco}	0.1	No dimension	(4)
Ratio of foraminifera to ZS	R_{fora}	0.1	No dimension	(4)
Ratio of inorganic carbon to total carbon in cocolithophorids	R_{Ccoco}	0.5	No dimension	(4)
Ratio of inorganic carbon to total carbon in foraminifera	R_{Cfora}	0.5	No dimension	(4)

Sources noted here are: (1) Yamanaka et al. (2004), (2) Chai et al. (2002), (3) this study, (4) Fujii et al. (2002), and (5) Suzuki and Takahashi (1995).

See Yoshie et al. (2005) for the model results of the biogeochemical responses to the iron enrichment at SEEDS using the observed physical forcings and the best-tuned biogeochemical parameter sets. Forced with either in situ or climatological temperature and salinity at each site and the solar radiation calculated from the zenith angle at each latitude (Numaguti, Takahashi, Nakajima, & Sumi, 1997), the model simulations are performed for 60 days starting from July 5 of 2001 at SEEDS, February 6 of 1999 at SOIREE,

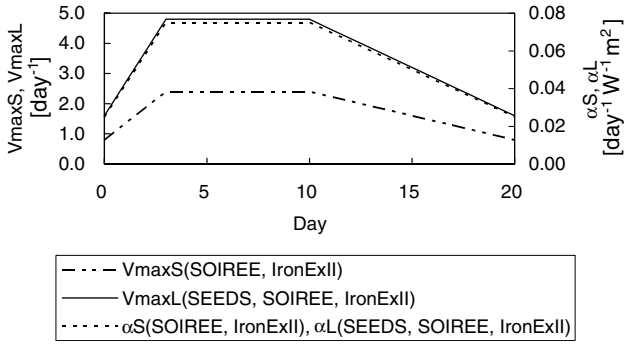

Fig. 2. Temporal changes of α_L [day^{-1} W^{-1} m^2] and $V_{max\,L}$ [day^{-1}] at SEEDS, SOIREE and IronExII, and α_S [day^{-1} W^{-1} m^2] and $V_{max\,S}$ [day^{-1}] at SOIREE and IronExII from Day 0 (July 18 of 2001 at SEEDS, February 9 of 1999 at SOIREE, and May 29 of 1995 at IronExII) in the model.

and May 26 of 1995 at IronExII. The temperature and salinity in the model are assumed unchanged after the final day of observation at each site, as is the procedure in Hannon et al. (2001). The solar radiation in the model is simply converted to the photosynthetically active radiation by multiplying by 0.45 (Moore, Doney, Kleypas, Glover, & Fung, 2002).

3. Results and discussion

3.1. Characteristics of the modeled biogeochemical responses to iron enrichments

Observed sea surface temperature increased by 2.2 °C from 7.4 to 9.6 °C at SEEDS during the iron-enrichment experiment period, due to increasing stratification of the surface waters in this season. It decreased by 0.8 °C from 2.1 to 2.9 °C at SOIREE during the experimental period, probably resulting from decrease in the wind speed (Bakker, Watson, & Law, 2001). It decreased by 1 °C from 25.2 to 24.2 °C at IronExII during the experimental period, reflecting a series of small mixing events with the deep water (Coale et al., 1996). These temperature changes are incorporated into the model by using the observations as input data (Fig. 3(a), (c) and (e)).

The calculated daily-averaged solar radiation reaches its annual maximum in June and December, and its annual minimum in December and June, in the Northern and Southern Hemisphere, respectively. At the equator, the annual maximum appears in March and September, and the annual minimum appears in June and December. During the simulation period of 60 days, it gradually decreases from 228 to 168 W m^{-2} at SEEDS, and from 135 to 84 W m^{-2} at SOIREE. At IronExII, it decreases from 173 W m^{-2} and then increases to 205 W m^{-2} with the minimum of 165 W m^{-2} in mid-June during the simulation period (Fig. 3(b), (d) and (f)). The values correspond to the in situ data or the climatological data (Bishop & Rossow, 1991) although the in situ data were highly variable with cloud cover.

The modeled, daily-averaged results of biogeochemical components without any temporal changes of the parameter values (corresponding to outside the iron patch) at each site are shown by the dotted lines in Figs. 4–6. Despite the decrease in the solar radiation at each site, the modeled phytoplankton biomass increases due to the temperature increase during the simulation period at SEEDS and SOIREE. As a result, the modeled surface chlorophyll-*a*, PP_{PS}, PP_{PL} and $PP_{PS} + PP_{PL}$ (PP_{total}) generally increase at SEEDS and SOIREE (Figs. 4(b), (c) and 5(b), (c)).

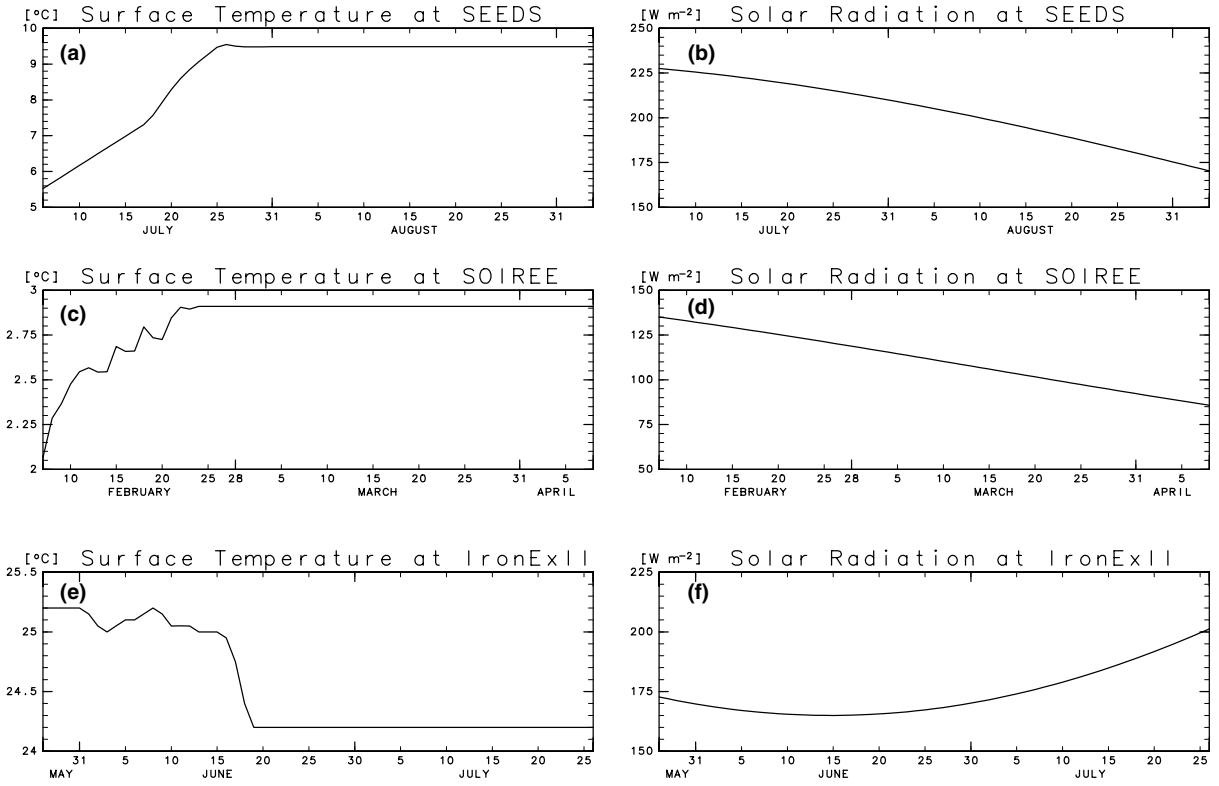

Fig. 3. Modeled daily-averaged surface temperature [°C] and solar radiation [W m^{-2}] at SEEDS ((a) and (b)), SOIREE ((c) and (d)), and IronExII ((e) and (f)) during the simulation period.

The model results with temporal changes of the parameter values as described in Fig. 2 (corresponding to inside the iron patch) at each site are shown by the solid lines in Figs. 4–6. The model results reproduce the observations well during all three in situ iron-enrichment experiments. For example, the model reproduces rapid increase in the surface chlorophyll-*a* of PL and the PP_{PL}, and decrease in surface nitrate, silicate and CO_2 fugacity at the sea surface ($(fCO_2)_{sea}$) after the iron infusion at SEEDS (Fig. 4(a), (b), (c) and (f)). The modeled surface chlorophyll-*a* of PS and the PP_{PS} also increase rapidly at SOIREE and IronExII (Figs. 5(b), (c) and 6(b), (c)), as well as PL and PP_{PL}. The modeled maximum of the PP_{total} appears at Days 8, 11 and 6 after the initial iron infusion at SEEDS, SOIREE and IronExII, respectively, which matches with the observations relatively well. The modeled maximum of the downward flux of POC at 100 m-depth (export production hereafter) and minimum of the $(fCO_2)_{sea}$ appear on Day 13 at SEEDS, Day 20 at SOIREE and Day 10 at IronExII, after the initial iron infusion. The model takes longer to reach maxima of surface ZL and ZP at each site, indicating that larger zooplankton need more time to respond to the iron enrichment. In general, the modeled maximum responses of the ecosystem to iron fertilization appear sooner after the iron infusion in warmer areas than colder regions (see Section 3.3 for discussion).

At SEEDS, only $V_{max\,L}$ and α_L change during the iron infusion (Fig. 2) because the observed small phytoplankton biomass increased only by a factor of 2–5 after the iron enrichment (Tsuda et al., 2003). At SOIREE and IronExII, on the other hand, both PS and PL increase significantly in the model because $V_{max\,S}$ and α_S are also changed by the iron infusion. The modeled maxima or minima of biogeochemical components are different among the sites. The modeled surface total chlorophyll-*a* and PP_{total}

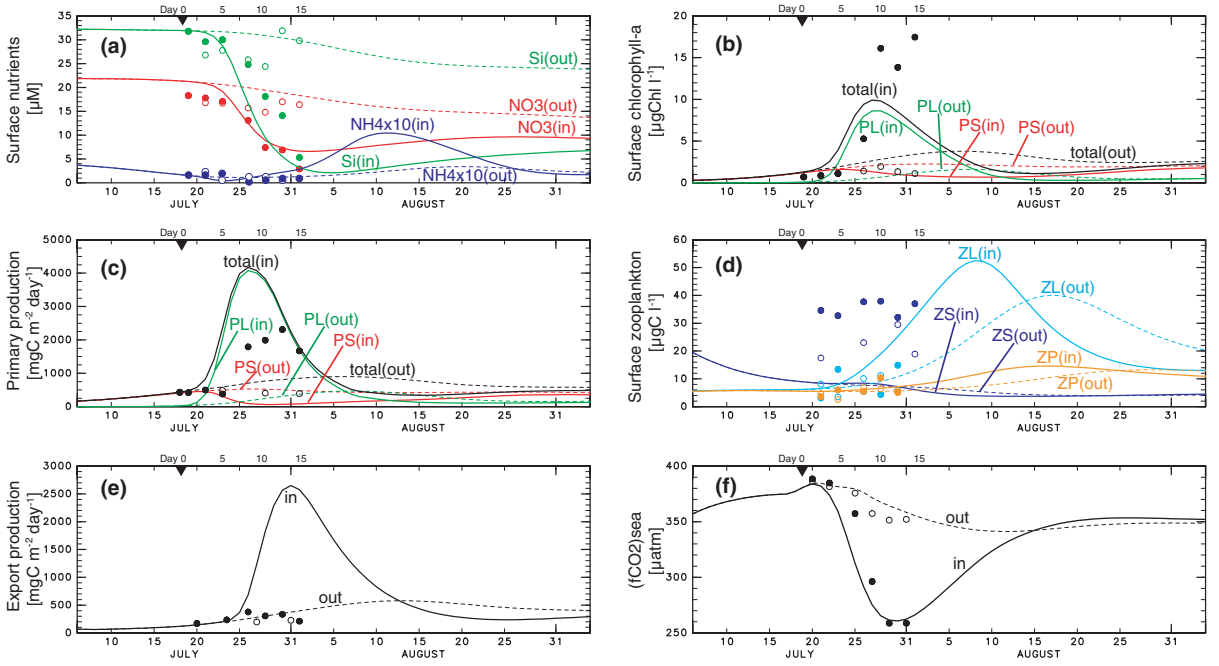

Fig. 4. Modeled daily-averaged results of (a) surface nitrate, silicate and ammonium (multiplied by ten for ammonium) [μM], (b) surface chlorophyll-*a* of PS, PL and total [μg Chl l^{-1}], (c) PP_{PS}, PP_{PL} and PP_{total} [mg C m^{-2} day^{-1}], (d) surface ZS, ZL and ZP [μg C l^{-1}], (e) export production [mg C m^{-2} day^{-1}] and (f) $(fCO_2)_{sea}$ [μatm] at SEEDS. Solid and dashed lines show the modeled values inside and outside the patch, respectively. Solid and open dots denote the field observation data inside and outside the patch, respectively. A solid triangle shows the date on which the iron was infused (Day 0).

are around 9.9 μg Chl l^{-1} and 4171 mg C m^{-2} day^{-1} at SEEDS, 1.9 μg Chl l^{-1} and 1186 mg C m^{-2} day^{-1} at SOIREE, and 1.8 μg Chl l^{-1} and 2778 mg C m^{-2} day^{-1} at IronExII (Figs. 4(b), (c), 5(b), (c) and 6(b), (c)). The values generally agree with the field observations, although the modeled surface chlorophyll-*a* is an underestimate and the modeled PP_{total} is an overestimate at SEEDS (Yoshie et al., 2005). The modeled surface chlorophyll-*a* is 5 times higher and the modeled PP_{total} is 1.5 and 3.5 times higher at SEEDS than at the other sites.

The modeled maximum of export production is 2650 mg C m^{-2} day^{-1} at SEEDS, 524 mg C m^{-2} day^{-1} at SOIREE and 393 mg C m^{-2} day^{-1} at IronExII (Figs. 4(e), 5(e) and 6(e)). The averaged e-ratio, defined as the export production over the PP_{total} during the simulation period, is estimated by the model as 0.50 at SEEDS, 0.41 at SOIREE and 0.12 at IronExII. The modeled POC at IronExII quickly recycles in the top 100 m, because the higher water temperature results in a higher remineralization rate in the model, as described in Eq. (3). Hence, the modeled e-ratio is much lower than for the other sites.

The modeled maxima of ZL and ammonium in the surface waters appear around three weeks after the initial iron infusion at SEEDS, more than one and half months after for SOIREE, but only 10 days after for IronExII. It consistently occurs well after the modeled maximum of PP_{total} (Figs. 4(a), (d), 5(a), (d) and 6(a), (d)). The biogeochemical components related to the heterotrophy, such as zooplankton biomass and ammonium that is mainly produced by zooplankton excretion, tend to be similar in terms of the magnitude of increase among the three sites. The modeled maximum values are 52.5, 19.9 and 29.5 μg C l^{-1} in the surface ZL, and 1.0, 0.4 and 0.7 μM in the surface ammonium at SEEDS, SOIREE and IronExII, respectively. The variation is only a factor of 2 or so among the sites. The difference is even smaller for the modeled maximum of surface ZP. The modeled maximum of surface ZP appears several days after

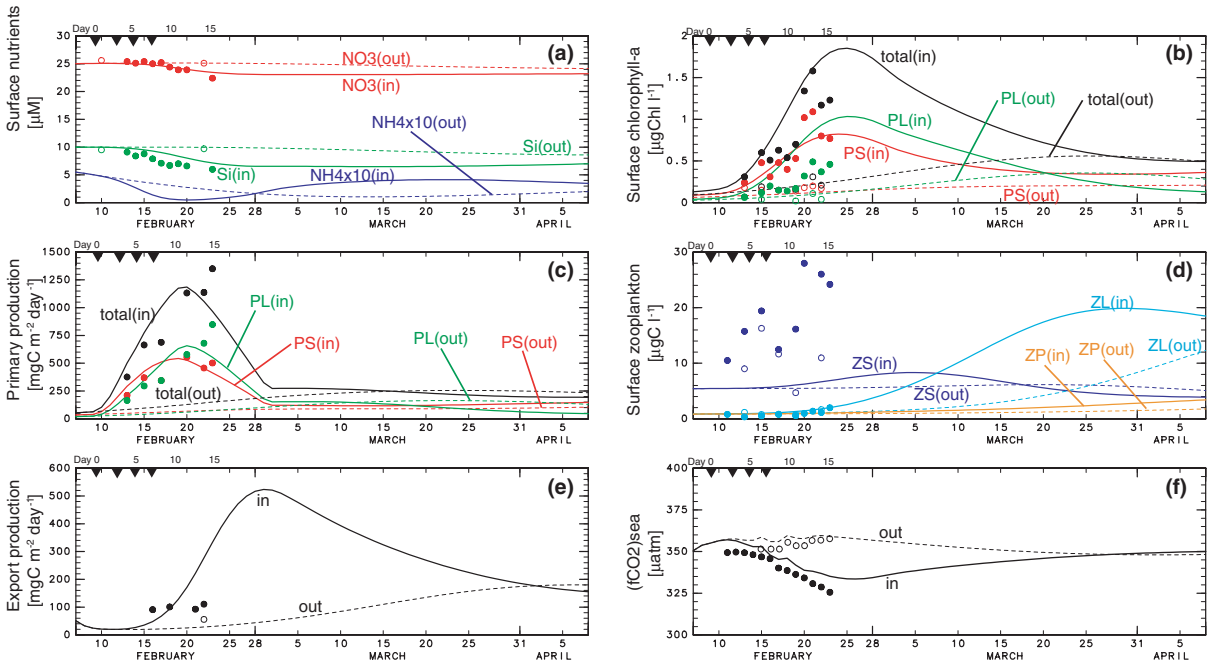

Fig. 5. Same as Fig. 4 but for SOIREE. Solid triangles show the dates in which the iron was infused (Days 0, 3, 5 and 7). Observational data are from Bakker et al. (2001), Charette and Buesseler (2000), Frew et al. (2001), Gall et al. (2001a, 2001b), Hall and Safi (2001), Nodder and Waite (2001) and Trull and Armand (2001).

the corresponding maximum of surface ZL appears at SEEDS and IronExII, but cannot be captured at SOIREE during the simulation period.

The modeled $(fCO_2)_{sea}$ rapidly decreases following the phytoplankton bloom (Figs. 4(f), 5(f) and 6(f)). The modeled minimum occurs just before the modeled maximum of export production at all sites. The modeled maximum of decrease in the $(fCO_2)_{sea}$ resulting from the iron enrichment during the experiment period, defined as the difference in $(fCO_2)_{sea}$ between outside and inside the iron patch, is estimated to be 103 μatm at SEEDS, 25 μatm at SOIREE and 46 μatm at IronExII. These values are close to the observed values of 94 μatm at SEEDS (Tsuda et al., 2003), 32 μatm at SOIREE (Bakker et al., 2001) and 73 μatm at IronExII (Steinberg, Millero, & Zhu, 1998), respectively.

The model captures most of the observed biogeochemical responses to the iron infusion at all sites. An exception is the export production at SEEDS and SOIREE. No significant increase of the export production is observed at the two sites. Tsuda et al. (2003) infer that a major part of the fixed carbon might stay in the surface mixed layer as POC at the end of the SEEDS observation, and that the observation is not long enough to capture increase in the export production. On the other hand, this discrepancy between the observation and simulation is also probably due to insufficiency of the biogeochemical model structure, because the discrepancy at SEEDS is lessened by separating diatoms into two groups in our ecosystem model (Yoshie et al., 2005).

The modeled magnitude and timing of maxima of biogeochemical components at SOIREE are different between this study and Hannon et al. (2001). For example, the modeled maximum of PP_{PL} in this study appears at Day 11 and the value is 650 mg C m^{-2} day^{-1}. The modeled maximum in Hannon et al. (2001), on the other hand, appeared later (at Day 27) and was 2820 mg C m^{-2} day^{-1}. Therefore, the two models lead to different conclusions, that is, the 13-day observation is apparently long enough to capture the maximum of

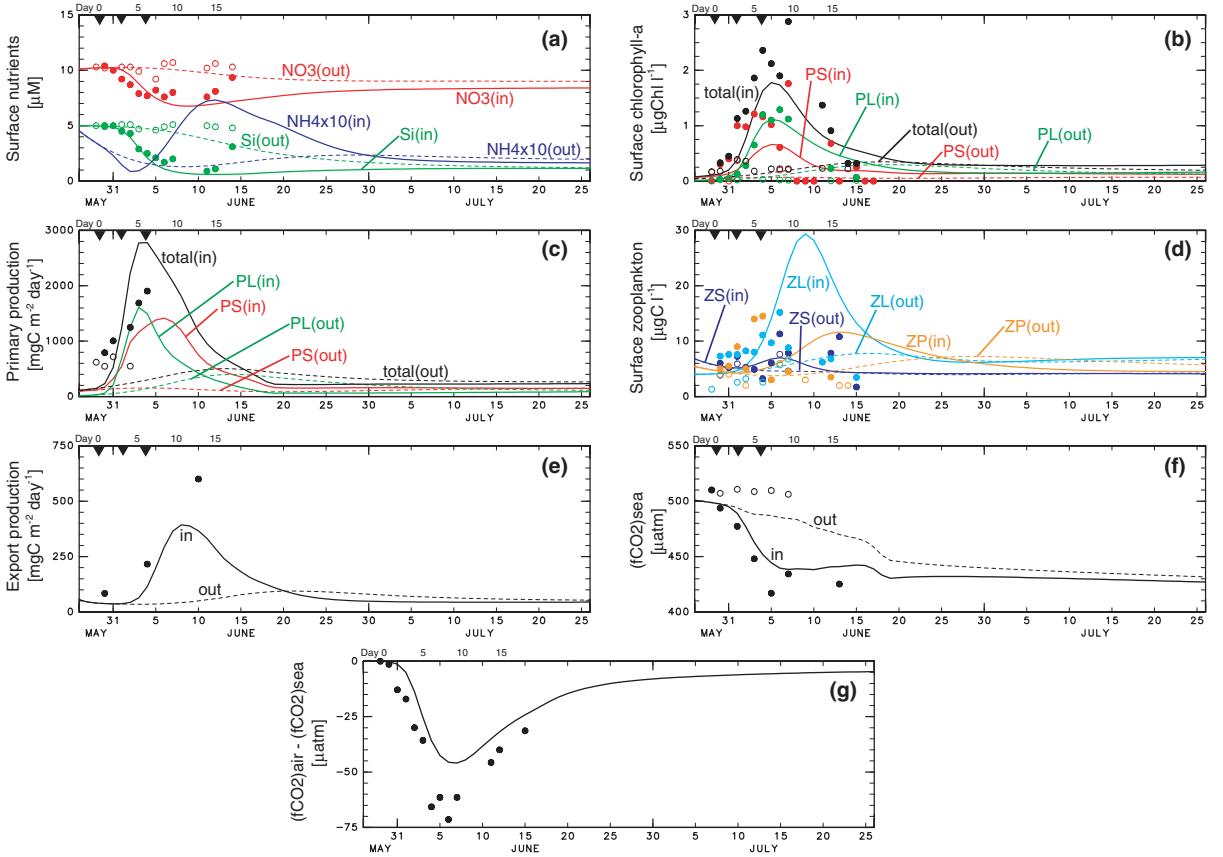

Fig. 6. Same as Fig. 4 but for IronExII. The modeled difference between $(fCO_2)_{air}$ and $(fCO_2)_{sea}$ (ΔfCO_2) is described in (g). Solid triangles show the dates on which the iron was infused (Days 0, 3 and 7). Observational data are from Coale et al. (1996), Cooper et al. (1996), Rollwagen Bollens and Landry (2000) and Landry et al. (2000).

PP_{PL} according to this study, but it was not captured by Hannon et al. (2001). The fundamental difference between these two modeling approaches is that we implicitly treat the iron limitation by changing values of the photosynthetic parameters as shown in Fig. 2, while Hannon et al. (2001) included the iron cycle explicitly in their model. To further understand the difference between these two approaches, we need to develop more advanced iron limitation and cycling models. Also, longer periods of field observations during the iron-fertilization experiments are needed for evaluation of results from both observations and models, particularly about physiology of the diatoms such as aggregation during the iron-induced bloom.

3.2. What other factors control biological productivity in the HNLC regions?

Recent open ocean iron-infusion experiments have demonstrated that iron is the dominant factor limiting photosynthesis in HNLC regions. Below, we use our model to examine the role of other factors in regulating the biological productivity at each site.

Fig. 7 shows time series of modeled vertically integrated regulating limitation factors on the PP_{PL} (nitrogenous nutrients, silicate, temperature and light) weighted by the PL biomass at each site. A higher value means weaker limitation on the diatom growth by each factor. The temperature limitation is

extremely weak at IronExII where the water temperature is relatively high. The light limitation is relatively strong at SOIREE because of low irradiance. The light limitation becomes stronger during the phytoplankton bloom inside the patch at all sites. This is due to self-shading by the phytoplankton that is consistent with the observations during the phytoplankton bloom (Boyd et al., 2000; Nelson & Smith, 1991; Saito & Tsuda, 2003; Saito, Tsuda, & Kasai, 2002). The silicate limitation becomes stronger inside the patch at

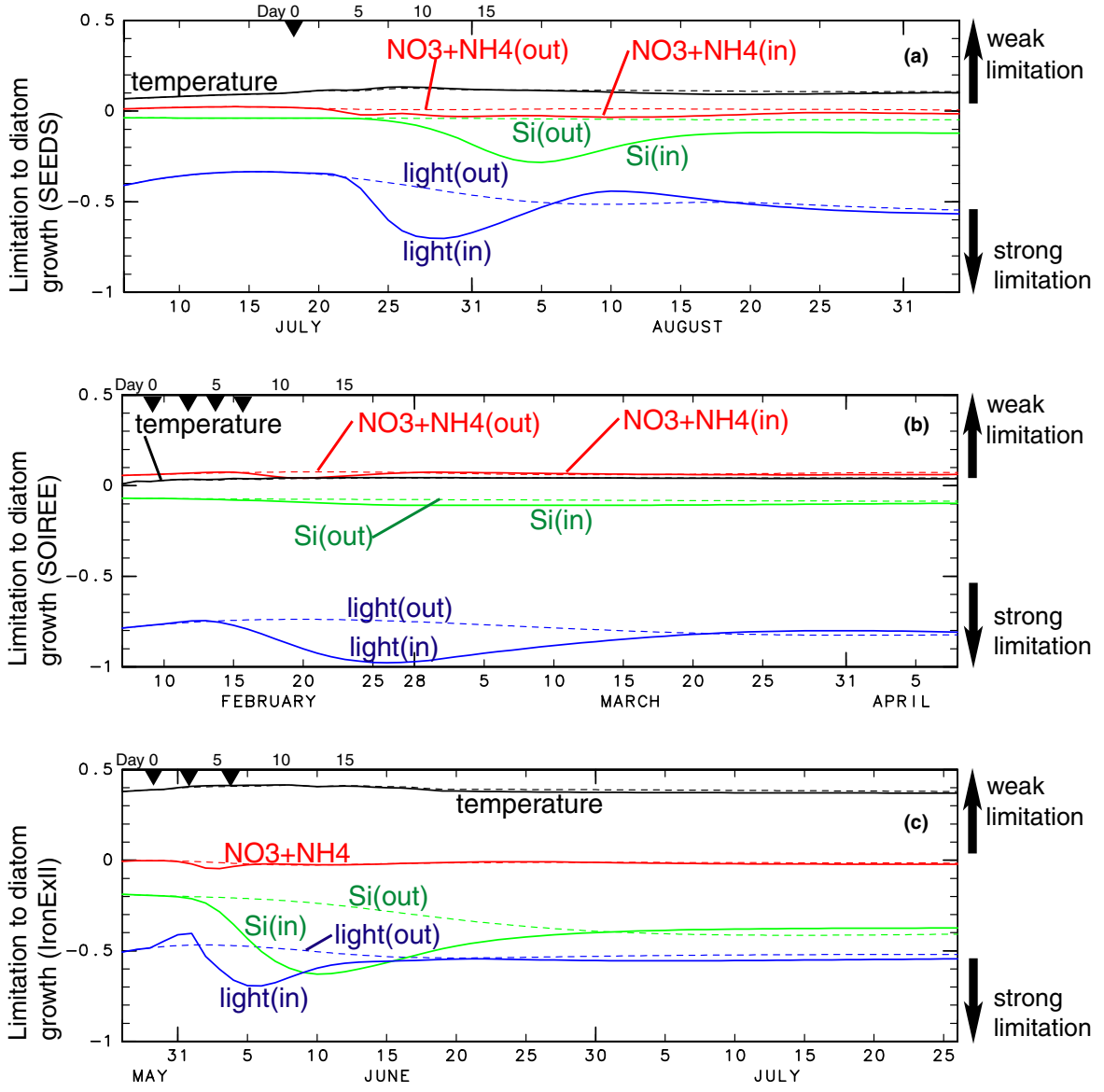

Fig. 7. Modeled daily-averaged common logarithm of the vertically integrated regulating limitation factors on the PP_{PL} (nitrogenous nutrients, silicate, temperature and light) weighted by the diatom biomass at (a) SEEDS, (b) SOIREE and (c) IronExII. Solid and dashed lines show the model results inside and outside the patch, respectively. Solid triangles show the date on which the iron was infused at each site.

SEEDS and IronExII during later phases of the blooms because the surface silicate concentration becomes lower than the k_{Si}. The limitation of nitrogen is not as strong as light and silicate throughout the simulation period at all sites. In summary, once the iron limitation is alleviated, the model results suggest that the PP_{PL} is strongly constrained by the silicate at IronExII and SEEDS, and that the light is a stronger limitation term at SOIREE.

3.3. Biogeochemical responses to duration of the iron enrichment

Duration of the iron infusion, i.e., the number of times iron was added and the duration of elevated iron concentration were different among the experiments: only a single iron release during SEEDS (on July 18 of 2001), and multiple releases during SOIREE (four times on February 9, 12, 14 and 16 of 1999) and during IronExII (three times on May 29, June 1 and 5 of 1995). Sensitivity studies of the ecosystem model to duration of the iron infusion seem useful for identifying which infusion protocol is the most effective in increasing export production and uptake of atmospheric CO_2. We examine this model sensitivity for the SEEDS simulation by setting the length of the duration for which α_L and $V_{max\,L}$ were kept at their highest levels to 3 days (case 1), 7 days (case 2; standard, see Fig. 2), 11 days (case 3) and 15 days (case 4).

Fig. 8 shows the model results of cases 1 through 4. The maxima of PP_{total} and export production in cases 2 through 4 are all similar, but they are all stronger and more persistent than in case 1. This is because the photosynthesis by diatoms that is the only phytoplankton group stimulated by the iron infusion at this site is strongly restricted by low surface silicate concentration after the bloom. The $(fCO_2)_{sea}$ in case 1 is not drawn down as low as in the other cases, all of which gave similar results. These model results suggest that at SEEDS multiple iron infusions can be more effective than a single iron infusion, but may not be as effective as generally expected because of strong silicate limitation on diatom growth. Multiple iron infusions, on the other hand, are more effective at SOIREE and IronExII than at SEEDS (not shown), because at these two sites PS could bloom after the PL bloom ceases due to the silicate limitation.

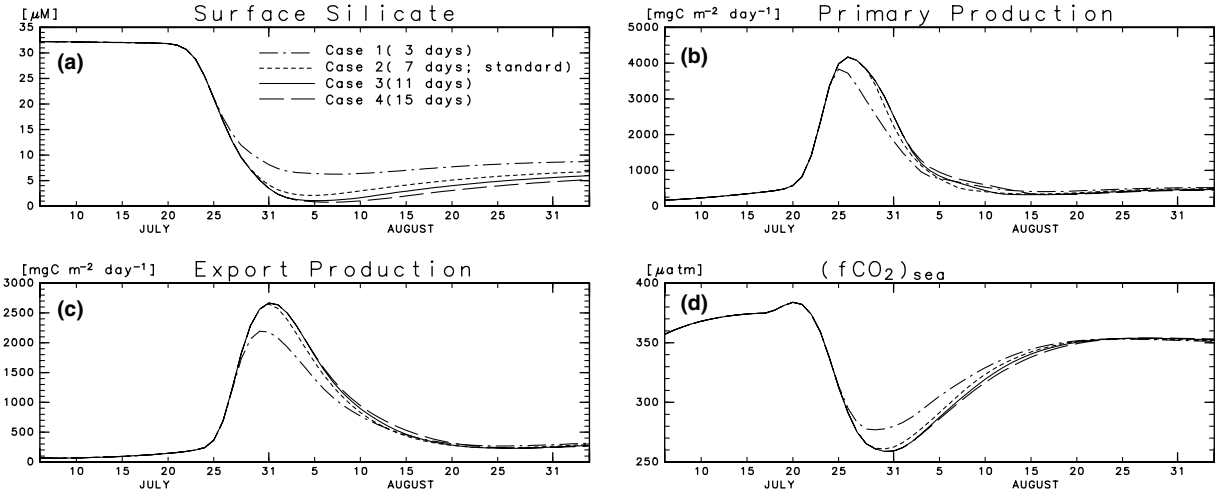

Fig. 8. Modeled daily-averaged results of (a) surface silicate [μM], (b) PP_{total} [mg C m^{-2} day^{-1}], (c) export production [mg C m^{-2} day^{-1}] and (d) $(fCO_2)_{sea}$ [μatm] at SEEDS in case 1 (dotted dashed lines), 2 (dotted lines), 3 (solid lines) and 4 (dashed lines), respectively.

3.4. Biogeochemical responses to difference of water temperature

It is essential to explore how water temperature affects biogeochemical processes during iron-infusion experiments, because the temperature in the mixed layer is notably different among the experiment sites. Here, we examine sensitivity of the biogeochemical processes to the water temperature at SEEDS by setting the temperature in the entire model domain to 0 °C (case 5), 5 °C (case 6), 10 °C (case 7), 15 °C (case 8), 20 °C (case 9) and 25 °C (case 10).

Fig. 9 shows the model results from cases 5 through 10. The maximum of PP_{total} appears earlier and is stronger as the temperature increases (Fig. 9(c)). This is because phytoplankton growth rate increases at higher temperatures. As a result, the maximum of PP_{total} is six days earlier and 2.4 times larger in case 10 than in case 5. However, the maximum of surface chlorophyll-*a* of PL is lower at higher temperatures (Fig. 9(a)), because of higher grazing pressure on PL at higher temperatures. The bloom terminates earlier at higher temperatures because of stronger silicate limitation on diatom growth (Fig. 9(a) and (b)). The export production also appears earlier at higher temperatures, 9 days earlier in case 10 than in case 5 (Fig. 9(d)). On the other hand, the maximum of the export production is lower at higher temperatures; at 25 °C (case 10) it is only a quarter of the highest value at 5 °C (case 6). This is because at higher temperatures the remineralization rate of POC becomes higher, and hence a larger fraction of the POC produced in the upper layer recycles before it sinks to the lower layer.

Fig. 10 shows the relationship among the PP_{total}, export production and e-ratio obtained by the simulations for SEEDS. Plots of the export production versus PP_{total} (Fig. 10(a)) indicate that the two components at the same temperature have a linear relationship and the gradient (equal to the e-ratio) is steeper at lower temperatures. Plots of the e-ratio versus PP_{total} (Fig. 10(b)) show that the e-ratio does not depend on PP_{total}, and that the e-ratio is more variable but higher at lower temperatures. These reports correspond to the model results presented in the previous section showing that the e-ratio is lower during IronExII.

Plots of the temperature versus e-ratio (Fig. 11) show good inverse correlation between the two components. The results agree both with previous observations and models (Laws, Falkowski, Smith, Ducklow, & McCarthy, 2000). The relation between temperature and e-ratio can be formulated by a linear function:

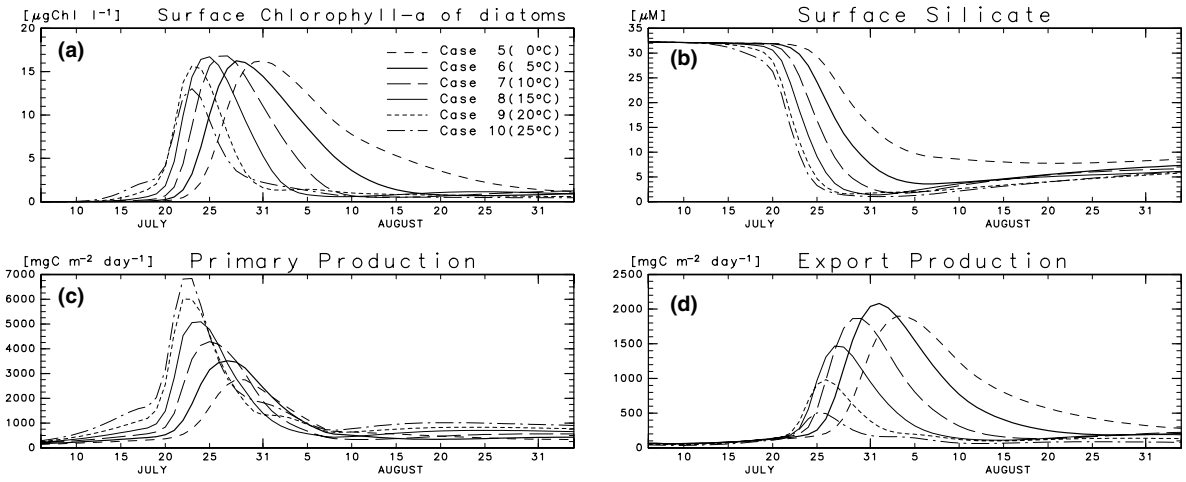

Fig. 9. Modeled daily-averaged results of (a) surface chlorophyll-*a* of PL, (b) surface silicate [μM], (c) PP_{total} [mg C m^{-2} day^{-1}] and (d) export production [mg C m^{-2} day^{-1}] at SEEDS in case 5 (heavy dashed lines), 6 (heavy solid lines), 7 (dashed lines), 8 (solid lines), 9 (dotted lines) and 10 (dotted dashed lines), respectively.

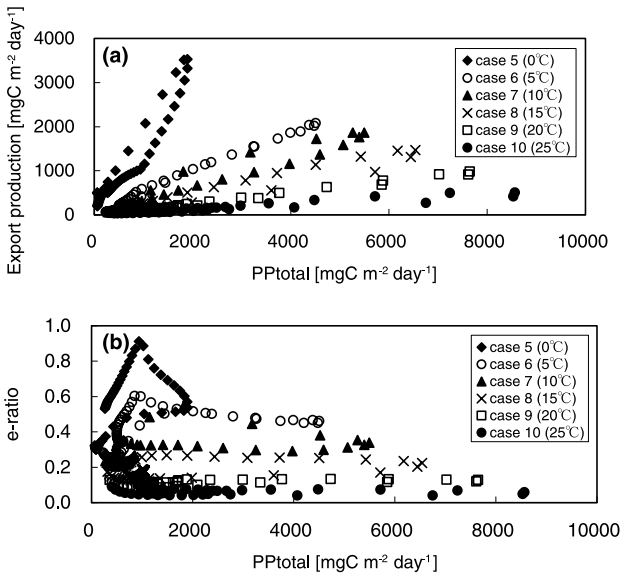

Fig. 10. Modeled plots of (a) PP_{total} [mg C m^{-2} day^{-1}] versus export production [mg C m^{-2} day^{-1}] and (b) PP_{total} [mg C m^{-2} day^{-1}] versus e-ratio at SEEDS in cases 5 through 10.

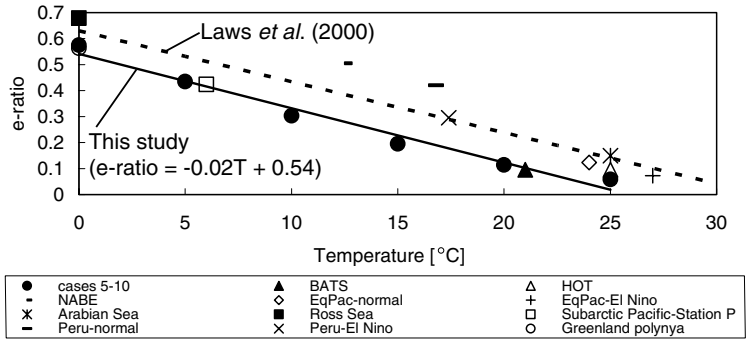

Fig. 11. Modeled plots of temperature versus the 60-day averaged e-ratio at SEEDS in cases 5 through 10. Reference data and the regression line from Laws et al. (2000) are also shown.

e-ratio = −0.02T + 0.54. A significant correlation coefficient of 0.98 between this function and the observed results strongly support a linear relation between temperature and e-ratio, as suggested by Laws et al. (2000).

From the model results above, we propose that the iron-infusion experiments can be most effective in generating export production in relatively cold water, say, 0 through 10 °C, assuming that other physical and biogeochemical conditions remain unchanged.

4. Summary

Using a fifteen-compartment marine ecosystem model, we examine biogeochemical responses to iron-enrichment experiments in three HNLC regions: SEEDS in the western North Pacific, SOIREE in the

Southern Ocean and IronExII in the Equatorial Pacific. The modeled biogeochemical components and processes at each site successfully reproduce the observations. Responses of the ecosystem to iron enrichment are relatively larger at SEEDS, earlier at IronExII and delayed at SOIREE. The e-ratio from the model during the simulation period is 0.50 at SEEDS, 0.41 at SOIREE and 0.12 at IronExII. The relatively lower e-ratio at IronExII is attributed to the higher recycling rate of POC in the warmer water. The modeled $(fCO_2)_{sea}$ drawdown is 103, 25 and 46 μatm at SEEDS, SOIREE and IronExII, respectively, close to the observations. These differences in model output result from differences in the physical environments such as the temperature and light, and in plankton species among the sites. Embedding more realistic processes of the iron limitation and cycle in the model, as well as longer-period observations to evaluate the model results, are required to reduce discrepancies in the results between observations and this study.

We examine other factors controlling biological productivity after the iron enrichment in the HNLC regions. The model results indicate that the diatom production is strongly constrained by light throughout the period at SOIREE and during the bloom at all sites due to self-shading by the phytoplankton. Silicate limitation is also strong at IronExII during later phase of the bloom. Model sensitivity studies on duration of the iron enrichment show that multiple iron infusions for longer than a week are not so effective at SEEDS because of the silicate limitation during later phase of the diatom bloom. From analysis of model sensitivity to the water temperature, we conclude that the export production (or e-ratio, the ratio of export production to primary production) has a negative linear correlation with temperature, and that the iron-enrichment experiments would become most effective for vertical export of carbon and atmospheric CO_2 drawdown where water temperature is colder than 10 °C. Thus, the model makes it possible to examine the region, timing and manner of new iron-enrichment experiments before they are carried out. Such ecosystem modeling is a useful tool for design of experiments and observational plans.

Acknowledgements

The authors wish to thank the SEEDS expedition group for providing observational data necessary for this study. We thank Drs. Jun Nishioka, Hiroaki Saito, Atsushi Tsuda, Mark Wells, and two anonymous reviewers for their constructive comments. Most of the figures were produced by the GFD-DENNOU Library.

References

Aita, M. N., Yamanaka, Y., & Kishi, M. J. (2003). Effect of ontogenetic vertical migration of zooplankton on the results of NEMURO embedded in a general circulation model. *Fisheries Oceanography, 12*, 284–290.

Bakker, D. C. E., Watson, A. J., & Law, C. S. (2001). Southern Ocean iron enrichment promotes inorganic carbon drawdown. *Deep-Sea Research Part II, 48*, 2483–2507.

Bishop, J. K. B., & Rossow, W. B. (1991). Spatial and temporal variability of global surface solar irradiance. *Journal of Geophysical Research, 96*, 16839–16858.

Boyd, P. W., Watson, A. J., Law, C. S., Abraham, E. R., Trull, T., Murdoch, R., et al. (2000). A mesoscale phytoplankton bloom in the polar Southern Ocean stimulated by iron fertilization. *Nature, 407*, 695–702.

Chai, F., Dugdale, R. C., Peng, T.-H., Wilkerson, F. P., & Barber, R. T. (2002). One-dimensional ecosystem model of the equatorial Pacific upwelling system. Part I: model development and silicon and nitrogen cycle. *Deep-Sea Research II, 49*, 2713–2745.

Chai, F., Jiang, M.-S., Barber, R. T., & Chavez, F. (submitted). Modeling iron enrichment in the equatorial Pacific Ocean. *Limnology and Oceanography*.

Charette, M. A., & Buesseler, K. O. (2000). Does iron fertilization lead to rapid carbon export in the Southern Ocean? Geochemistry Geophysics Geosystems, 1, Paper number 2000GC000069.

Coale, K. H., Johnson, K. S., Fitzwater, S. E., Gordon, R. M., Tanner, S., Chavez, F. P., et al. (1996). A massive phytoplankton bloom induced by an ecosystem-scale iron fertilization experiment in the equatorial Pacific Ocean. *Nature, 383*, 495–501.

Cooper, D. J., Watson, A. J., & Nightingale, P. D. (1996). Large decrease in ocean-surface CO_2 fugacity in response to *in situ* iron fertilization. *Nature, 383*, 511–513.

Frew, R., Bowie, A., Croot, P., & Pickmere, S. (2001). Macronutrient and trace-metal geochemistry of an in situ iron-induced Southern Ocean bloom. *Deep-Sea Research Part II, 48*, 2467–2481.

Fujii, M., Nojiri, Y., Yamanaka, Y., & Kishi, M. J. (2002). A one-dimensional ecosystem model applied to time-series Station KNOT. *Deep-Sea Research Part II, 49*, 5441–5461.

Gall, M. P., Boyd, P. W., Hall, J., Safi, K. A., & Chang, H. (2001a). Phytoplankton processes. Part 1: Community structure the Southern Ocean Iron RElease Experiment (SOIREE). *Deep-Sea Research Part II, 48*, 2551–2570.

Gall, M. P., Strzepek, R., Maldonado, M., & Boyd, P. W. (2001b). Phytoplankton processes. Part 2: Rates of primary production and factors controlling algal growth during the Southern Ocean Iron release Experiment (SOIREE). *Deep-Sea Research Part II, 48*, 2571–2590.

Hall, J. A., & Safi, K. (2001). The impact of in situ Fe fertilization on the microbial food web in the Southern Ocean. *Deep-Sea Research Part II, 48*, 2591–2613.

Hannon, E., Boyd, P. W., Silvoso, M., & Lancelot, C. (2001). Modeling the bloom evolution and carbon flows during SOIREE: Implications for future in situ iron-enrichments in the Southern Ocean. *Deep-Sea Research Part II, 48*, 2745–2773.

Landry, M. R., Ondrusek, M. E., Tanner, S. J., Brown, S. L., Constantinou, J., Bidigare, R. R., et al. (2000). Biological response to iron fertilization in the eastern equatorial Pacific (IronEx II). I. Microplankton community abundances and biomass. *Marine Ecology Progress Series, 201*, 27–42.

Laws, E. A., Falkowski, P. G., Smith, W.O. Jr., Ducklow, H., & McCarthy, J. J. (2000). Temperature effects on export production in the open ocean. *Global Biogeochemical Cycles, 14*, 1231–1246.

Martin, J. H. (1990). Glacial-interglacial CO_2 change: the iron hypothesis. *Paleoceanography, 5*, 1–13.

Moore, J. K., Doney, S. C., Kleypas, J. A., Glover, D. M., & Fung, I. Y. (2002). An intermediate complexity marine ecosystem model for the global domain. *Deep-Sea Research Part II, 49*, 403–462.

Nelson, D. M., & Smith, W. O. Jr., (1991). Sverdrup revisited: Critical depths, maximum chlorophyll levels, and the control of Southern Ocean productivity by the irradiance-mixing regime. *Limnology and Oceanography, 36*, 1650–1661.

Nodder, S. D., & Waite, A. M. (2001). Is Southern Ocean organic carbon and biogenic silica export enhanced by iron-stimulated increases in biological production? Sediment trap results from an in situ iron enrichment experiment. *Deep-Sea Research Part II, 48*, 2681–2701.

Numaguti, A., Takahashi, M., Nakajima, T., & Sumi, A. (1997). Description of CCSR/NIES atmospheric general circulation model (pp. 1–48). CGER's Supercomputer Monograph Report, Center for Global Environmental Research, National Institute for Environmental Studies, Tsukuba, Japan, 3.

Platt, T., Gallegos, C. L., & Harrison, W. G. (1980). Photoinhibition of photosynthesis in natural assemblages of marine phytoplankton. *Journal of Marine Research, 38*, 687–701.

Ridgwell, A. J. (2000). Climatic effect of Southern Ocean Fe fertilization: Is the jury still out? Geochemistry, Geophysics, Geosystems, 1, Paper number 2000GC000120.

Rollwagen Bollens, G. C., & Landry, M. R. (2000). Biological response to iron fertilization in the eastern equatorial Pacific (IronEx II). II. Mesozooplankton abundance, biomass, depth distribution and grazing. *Marine Ecology Progress Series, 201*, 43–56.

Saito, H., Suzuki, K., Hinuma, A., Ota, T., Fukami, K., & Kiyosawa, H., et al. (2005). Response of microzooplankton to in situ iron fertilization in the western subartic Pacific (SEEDS). *Progress in Oceanography*, doi:10.1016/j.pocean.2005.02.010.

Saito, H., & Tsuda, A. (2003). Influence of light intensity on diatom physiology and nutrient dynamics in the Oyashio region. *Progress in Oceanography, 57*, 251–263.

Saito, H., Tsuda, A., & Kasai, H. (2002). Nutrient and plankton dynamics in the Oyashio region of the western subarctic Pacific Ocean. *Deep-Sea Research Part II, 49*, 5463–5486.

Steele, J. H. (1962). Environmental control of photosynthesis in sea. *Limnology and Oceanography, 7*, 137–150.

Steinberg, P. A., Millero, F. J., & Zhu, X. (1998). Carbonate system response to iron enrichment. *Marine Chemistry, 62*, 31–43.

Suzuki, Y., & Takahashi, M. (1995). Growth responses of several diatom species isolated from various environments to temperature. *Journal ofPhycology, 31*, 880–888.

Trull, T. W., & Armand, L. (2001). Insights into Southern Ocean carbon export from the $\delta^{13}C$ of particles and dissolved inorganic carbon during the SOIREE iron release experiment. *Deep-Sea Research Part II, 48*, 2655–2680.

Tsuda, A., Kiyosawa, H., Kuwata, A., Mochizuki, M., Shiga, N., & Saito, H., et al. (2005). Responses of diatoms to iron-enrichment (SEEDS) in the western subarctic Pacific, temporal and spatial comparisons. *Progress in Oceanography*, doi:10.1016/j.pocean.2005.02.008.

Tsuda, A., Takeda, S., Saito, H., Nishioka, J., Nojiri, Y., Kudo, I., et al. (2003). A mesoscale iron enrichment in the western subarctic Pacific induces a large centric diatom bloom. *Science, 300*, 958–961.

Yamanaka, Y., Yoshie, N., Fujii, M., Aita, M. N., & Kishi, M. J. (2004). An ecosystem model coupled with nitrogen-silicon-carbon cycles applied to Station A7 in the northwestern Pacific. *Journal of Oceanography, 60*, 227–241.

Yoshie, N., Fujii, M., & Yanamaka, Y. (2005). Ecosystem changes with the iron fertilization in the western North Pacific simulated by a one-dimensional ecosystem model. *Progress in Oceanography*, doi:10.1016/j.pocean.2005.02.014.